Chinese Journal of
POLYMER SCIENCE

RESEARCH ARTICLE

https://doi.org/10.1007/s10118-022-2678-4
Chinese J. Polym. Sci. **2022**, *40*, 345–354

Construction of Safety and Non-flammable Polyimide Separator Containing Carboxyl Groups for Advanced Fast Charing Lithium-ion Batteries

Ji-Ping Gu, Kai-Yuan Zhang, Xiu-Ting Li, Jie Dong, Qing-Hua Zhang, and Xin Zhao*

State Key Laboratory for Modification of Chemical Fibers and Polymer Materials, College of Materials Science and Engineering, Donghua University, Shanghai 201620, China

Electronic Supplementary Information

Abstract With the wide applications of lithium-ion batteries (LIBs) in electronic devices and electric vehicles, it is of great importance to improve their safety and electrochemical performance. Herein, soluble polyimides (PI) containing carboxyl groups (—COOH) were synthesized by a simple one-step method and PI separators with sponge-like, interpenetrating porous structures were prepared *via* non-solvent induced phase separation (NIPS). The obtained PI separators exhibited excellent thermal stability and fire-resistance properties, with the electrolyte uptake of 344% and good dimensional integrity in air at 200 °C. The results showed that the lithium-ion transference number of the obtained PI separator could reach 0.48, which was much higher than that of the Celgard-2400 separator (0.38). The Li/$LiFePO_4$ half-cell with the PI separator showed excellent cycle capability and high-rate performance with a high capacity of 121.80 mA·h·g^{-1} at 5 C, which was better than that of the cell with the Celgard-2400 separator (54.3 mA·h·g^{-1}), demonstrating the promising applications of this PI separators in LIBs.

Keywords Polyimide; Separator; Carboxyl groups; Non-solvent induced phase separation; Li transference number

Citation: Gu, J. P.; Zhang, K. Y.; Li, X. T.; Dong, J.; Zhang, Q. H.; Zhao, X. Construction of safety and non-flammable polyimide separator containing carboxyl groups for advanced fast charing lithium-ion batteries. *Chinese J. Polym. Sci.* **2022**, *40*, 345–354.

INTRODUCTION

As environmental concerns grow, sustainable energy sources will gradually replace fossil fuels as the future trend, such as solar, wind and tidal energy.[1] Among various energy storage devices, lithium-ion batteries are widely used in portable electronic products, such as rechargeable batteries for mobile phones, laptops, video cameras, and as a power source for electric vehicles, due to their high energy density, long cycling life, low self-discharge rate and low memory effect.[2–5] The separators act as a physical barrier in lithium-ion batteries, preventing direct contact between the anode and cathode, while allowing rapid transport of lithium ions.[6–8]

Currently, commercial polyolefin separators, such as polypropylene, polyethylene and their composite separators, are widely used, which have good mechanical properties, stable chemical properties and low prices.[9–11] However, the non-polar nature of polyolefins and their low porosity result in poor wettability with polar electrolytes.[12] In addition, the poor thermal stability of polyolefin separators leads to thermal shrinkage or even melting under conditions such as overcharging or heating, resulting in short-circuiting of the battery, which poses certain safety hazards.[13–16] In order to solve the inherent shortcomings of polyolefin separators, researchers have turned their attention to highly heat-resistant polymers[17] such as polybenzimidazole (PBI),[18–20] aramid nanofiber (ANF),[21–23] polyetherimide (PEI),[24–26] poly(phthalazinone ether sulfone ketone) (PPESK)[27] and polyimide (PI).[28–31] As we all know, aromatic polyimide has excellent chemical and thermal stability and low dielectric constant, implying that PI is a good candidate with great potentials as separator materials for lithium-ion battery.[32] Dong *et al.*[33] reported PI-titanium dioxide (TiO_2) core-shell nanofibrous membrane *via* the electrospinning technique, which exhibited good thermal dimensional stability and excellent electrolyte absorption even at 300 °C. However, the presence of the TiO_2 layer inevitably increases the diameter of the nanofibers, leading to a reduction in the porosity and electrolyte uptake of the PI separators. Moreover, there is a risk of nanoparticle shedding during long battery cycling which may weaken the cycling performance of the battery. It is worth noting that the separators prepared by electrospinning technique usually have large pore sizes prone to self-discharge and short circuits caused by lithium dendrite growth.[34–37] Kong *et al.*[26] prepared PEI separators by electrostatic spinning, the maximum pore size of the separator could reach more than 5 μm

* Corresponding author, E-mail: xzhao@dhu.edu.cn

Received October 25, 2021; Accepted December 9, 2021; Published online February 15, 2022

and the fibers were loosely and randomly stacked together with a mechanical strength of only 4 MPa, which resulted in lithium dendrites easily puncturing the separator leading to short circuits. Although Kong *et al*. used an *in situ* melting method to bond the fibers to each other thereby reducing the pore size and increasing the mechanical strength, this was accompanied by a decrease in porosity and electrolyte uptake. In recent years, phase conversion has been considered to be an effective method for preparing separators with controlled porous structures. The phase inversion process is thermodynamically and kinetically controllable and therefore allows to form pores with the appropriate morphology and size.[38] Zhang *et al*.[39] prepared porous PI separators from poly(amide acid) (PAA) *via* non-solvent induced phase separation (NIPS) and thermal imidization process. By controlling the NIPS process, PI separators with high porosity and pore connectivity were successfully obtained. And the average pore size of the PI-40 separator is 0.62 μm, with most pores being less than 1 μm.

On the other hand, lithium-ion transport properties have an important impact on the high performance of lithium-ion batteries. To improve the lithium-ion transport performance, several polymeric materials with charged functional groups have been used in the design of separators. Li *et al*.[40] synthesized a unique sulfonated aromatic heterocyclic polymer with $-SO_3$ groups, which allowed positively charged Li^+ to pass through while preventing anions movement by electrostatic repulsion, thereby increasing the lithium ion transference number. With the $-SO_3$ groups, the −COOH containing unshared electron pairs can interact with Li^+ in the solvent and promote the transfer of Li^+. Lin *et al*.[41] introduced the −COOH groups to the surface of the PI separator by alkali etching. The obtained carboxylated PI separator facilitated an increase in the lithium-ion transference number (up to 0.87), which was four times higher than that of the original PI separator. However, this alkali etching method inevitably sacrifices the mechanical properties of the PI separator.

In this work, soluble PI containing carboxyl groups (−COOH) were prepared by a one-step method. The porous PI separators were prepared by the NIPS process. On the one hand, the influence of the solidification bath composition on the pore structures of the separator has been investigated and the mechanical, thermal and electrochemical properties of the separator are discussed. On the other hand, without degrading the mechanical properties, the effect of the introduction of the −COOH groups on the lithium-ion transport properties is analyzed.

EXPERIMENTAL

Materials

N-methyl-2-pyrrolidone (NMP) obtained from Sinopharm Chemical Reagent Co., Ltd. was directly used as received. 4,4′-Oxydiphthalic anhydride (ODPA) was purchased from Sinopharm Chemical Reagent Co., Ltd. and used without further purification. 2,2'-Bis(trifluoromethyl)benzidine (TFMB) and 3,5-diaminobenzoic acid (DABA) were purchased from Changzhou Sunlight Pharmaceutical Co., Ltd. and used directly. The liquid electrolyte (1 mol/L $LiPF_6$ in ethylene carbonate (EC)/dimethyl carbonate (DMC)/ethyl methyl carbonate (EMC) (1:1:1, *W*:*W*:*W*)) was obtained from Nanjing Morges Energy Technology Co., Ltd. The commercial PE separator (Celgard 2400, Asahi Kasei, Japan) with a thickness of approximately 25 μm was used for comparison as a separator for LIB.

Synthesis of Fluorinated Polyimides Containing Carboxyl Groups

PI was synthesized from dianhydride (ODPA) and diamine (TFMB and DABA) in equimolar ratios by a one-step high temperature polycondensation process in which the molar ratio of the two different diamines was 1:1, as shown in Fig. 1(a). In a typical experiment, NMP (93 mL), TFMB (4.8035 g, 0.015 mol) and DABA (2.2826 g, 0.015 mol) were sequentially added to a three-necked flask fitted with a condenser tube under nitrogen gas and stirred at low speed until dissolved. Subsequently, ODPA (9.3063 g, 0.03 mol) was added. Then the solution was heated to 195 ℃ and maintained for 12 h. At the end of the reaction, an orange-red viscous liquid of soluble PI solution with a solid content of 15% was obtained and stored for use.

Fabrication of PI Membrane

The porous PI separators were prepared *via* a typical nonsolvent induced phase separation (NIPS) method. The viscous PI solution was diluted to a certain viscosity. As shown in Fig. 1(b), the solution was cast onto a clean glass plate using a squeegee with the thickness of 100 μm to form a liquid-like membrane. After that, the membrane was immersed into a solidifying bath containing of NMP and deionized water for 3 h and the membrane was then immersed in deionized water for further 24 h to remove any residual solvents. Subsequently, the obtained wet membrane was dried in a vacuum oven at 100 ℃ for 12 h to remove the water. In the NIPS process, the pore morphology was regulated by modulating the amount of NMP in the solidification bath.

Characterizations

The chemical composition of the separators was characterized by Fourier transform infrared spectroscopy (ATR-FTIR, Nicolet 8700) and nuclear magnetic resonance (^{1}H-NMR) spectroscopy (Bruker Avance 600) using DMSO-d_6 as solvent. The thermal stability of the separators was tested on a Netzsh 209F3 thermogravimetric analysis (TGA). Before TGA test, the dried membranes were further placed in a vacuum drying oven at 250 ℃ for 3h to remove residual NMP. The surface and cross-sectional morphologies of the separators were observed by field emission scanning electron microscopy (SEM-7800F). Mechanical properties were tested by an Instron 5969 instrument with a loading rate of 10 mm/min and a minimum of 10 samples measured per specimen. The wettability of the separators to the electrolyte was characterized by a contact angle goniometer (OCA40, Dataphysics). The porosity (*P*) of the separators was measured by the *n*-butanol method. In detail, PI samples with a certain size were immersed in *n*-butanol for 2 h and the mass of the PI samples before and after entry were recorded. The porosity of the samples was calculated according to the following Eq. (1):

$$P(\%) = \frac{(m_w - m_d)}{\rho \times V} \quad (1)$$

where m_d and m_w are the masses of the sample before and after 2 h immersion in *n*-butanol, respectively, ρ is the density of *n*-butanol and *V* is the volume of the sample.

https://doi.org/10.1007/s10118-022-2678-4

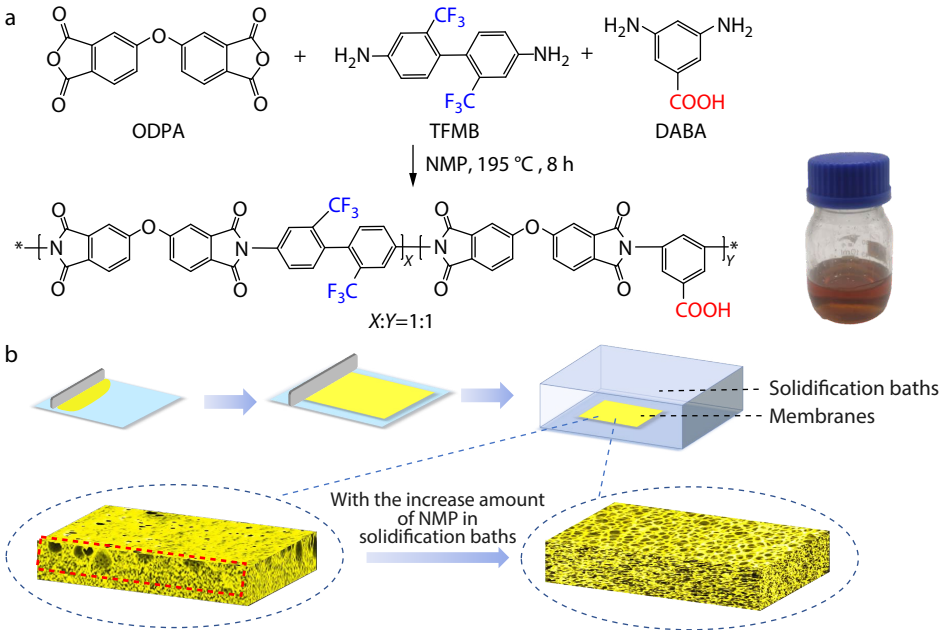

Fig. 1 (a) Synthesis of organo-soluble polyimide; (b) Schematic diagram of the fabrication procedure of PI separators.

The electrolyte uptake (EU) of the separators were determined using Eq. (2):

$$EU\,(\%) = (m_t - m_0)/m_0 \quad (2)$$

where m_0 and m_t are the weight of samples before and after 2 h immersion in 1 mol/L $LiPF_6$ solution, respectively.

Electrochemical Characterization

The ionic conductivity (σ) was calculated according to Eq. (3):

$$\sigma = L/(R_b \times A) \quad (3)$$

where L, R_b, A are the thickness of separators, bulk resistance (Ω) and effective area, respectively. The R_b value was measured from the AC impedance by using a CHI 600E electrochemical workstation (Chenhua, China) over a frequency range of 0.1 Hz to 100 kHz with an amplitude of 5 mV using a cell with the assembly of stainless steel (SS)/separator-liquid electrolyte/SS. The interfacial resistance (R_{int}) of the cell with the assembly of Li/separator-liquid electrolyte/Li was determined the same way as that of R_b. Afterwards the interfacial impedance of cell assembled from Li/separator-liquid electrolyte/$LiFePO_4$ was determined by AC impedance measurements with an amplitude of 5 mV over a frequency range of 0.01 Hz to 100 kHz. The electrochemical stability of the separators was tested *via* linear sweep voltammetry (LSV) using a SS/separator-liquid electrolyte/Li cell with the potential ranging from 3.0 V to 7.0 V at the sweep rate of 10 mV·s^{-1}. The lithium-ion transference number (t_{Li^+}) was calculated using Eq. (4):

$$t_{Li^+} = I_{ss}(\Delta V - I_0R_0)/I_0(\Delta V - I_{ss}R_{ss}) \quad (4)$$

where I_0 and I_{ss} represent the initial and steady-state currents, respectively. ΔV is the polarization potential (10 mV). R_0 and R_{ss} are the interface resistances before and after polarization, respectively. A coin-type half-cell consisted of $LiFePO_4$/separator-liquid electrolyte/lithium metal was used to study the performance for batteries. The cathode consisted of a mixture of active material ($LiFePO_4$ from Sigma Aldrich), conductive additive of acetylene black (AB) and the binder of PVDF at a mass ratio of 8:1:1. The cycle test was carried out at a fixed charge/discharge current density of 1 C/1 C between 2.0 V and 4.2 V. In addition, to further investigate the rate capability of the cells, the charge/discharge current density was varied between 0.2 C and 5.0 C. All cell assemblies were carried out in an argon filled glove box.

RESULTS AND DISCUSSION

Chemical Structures of PI Separators

Most aromatic polyimides are insoluble in most organic solvents due to their strong intermolecular interactions and the rigidity of their molecular chains. For this reason, polyimide materials are mainly obtained by processing PAA intermediate. However, PAA intermediates are unstable with aqueous byproducts emitting during the imidization process.[42] In particular, after phase conversion to separators, large volume shrinkage and molecular weight degradation can be expected during thermal imidization due to the poor thermal stability of the PAA. In order to overcome the disadvantages of PAA, soluble polyimides basedonthestructureofODPA-TFMB/DABAweresynthesized.Basically, the existence of flexible ether bonds and trifluoromethyl groups could reduce the chain rigidity and weaken the interchain interaction.[43] The introduction of the third component of DABA breaks the symmetry of the polymer chains and provides good solubility. While the carboxyl groups in DABA is expected to facilitate the migration of lithium ions.[41]

The chemical structures of the synthesized polyimide were characterized by FTIR and ^{1}H-NMR spectroscopy. In the FTIR spectrum as shown in Fig. 2(a), the characteristic absorption bands of imide-ring can be observed near 1785 cm^{-1} for asymmetric C=O stretching, 1725 cm^{-1} for symmetric C=O stretching, 1385 cm^{-1} for C—N—C stretching and 725 cm^{-1} for C=O bending. Moreover, the spectrum also displays the C—F stretching absorption band near 1121 cm^{-1}. At the same time, it can be observed in the spectrum that there is a broad

weak absorption peak at 3200–3500 cm^{-1}, which could be attributed to the vibration band of —COOH in the DABA fraction.[44] To further characterize the polyimide structure, a clear downfield proton signal at 13.5 ppm (H-a) can be observed in the ^{1}H-NMR spectrum as shown in Fig. 2(b), which is attributed to the —COOH group in DABA. At the same time, to further determine the chemical shift of H on the benzene ring in DABA, the ^{1}H-NMR hydrogen spectra containing DABA monomer were compared with those without DABA monomer (Fig. S1 in the electronic supplementary information, ESI), and it was found that with the introduction of DABA, new peaks appeared at 8.14 ppm (H-a) and 8.10 ppm (H-a), corresponding to H at the neighbouring and opposite positions on DABA monomer, respectively. This indicates the involvement of DABA monomer in the reaction, proving the carboxyl group-containing synthesis of polyimide.

Morphology and Electrolyte Wettability of PI Separators

The morphologies of porous PI separators prepared in solidification baths with different volume ratios of NMP/water were investigated. As shown in Fig. 3, a finger-like pore structure was formed with the ratio of NMP/water of 1:1 as coagulation bath (Fig. S2a in ESI). During the phase transition, the polymer solvent (NMP) diffused into the solidification bath and the non-solvent (water) diffused into the wet cast film. The rate of diffusion of solvent and non-solvent had a significant effect on the porous structure of the separators. As the NMP content in the solidification bath increased with the water content declining, the cross-sectional pore structures of the separator transferred from finger-like to sponge-like morphologies. This is because as the amount of good solvent (NMP) in the solidification bath increases, the tendency for the non-solvent (H_2O) to diffuse into the polymer solution slows down; therefore, more time is needed to complete the liquid-liquid phase separation process, which results in a delay in demixing. Typically, the instant delamination processes tended to result in large pores and finger-like structures, while delayed delamination processes usually resulted in sponge-like structures.[39] The film displays a dense sponge-like pore structure when the NMP content in the solidification bath is above 82%. As shown in Table 1, the

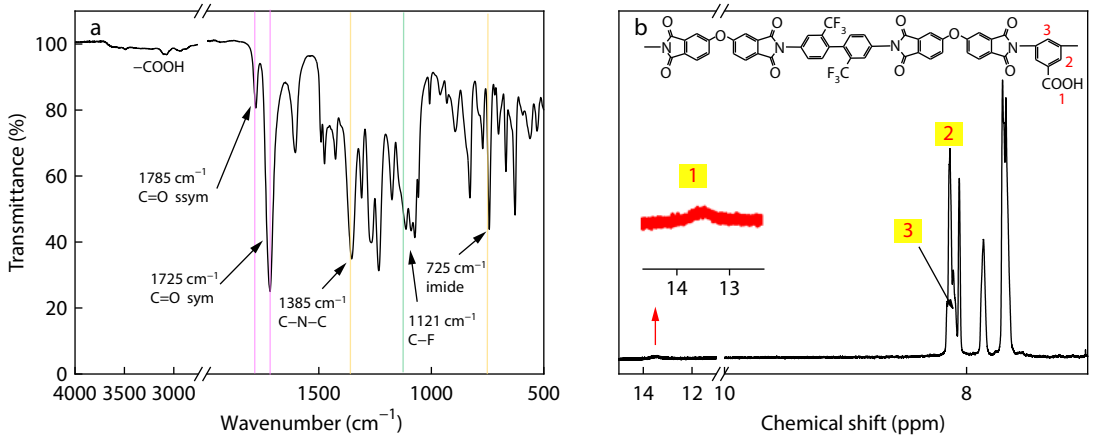

Fig. 2 (a) FTIR spectrum and (b) ^{1}H-NMR spectrum of the synthesized polyimide.

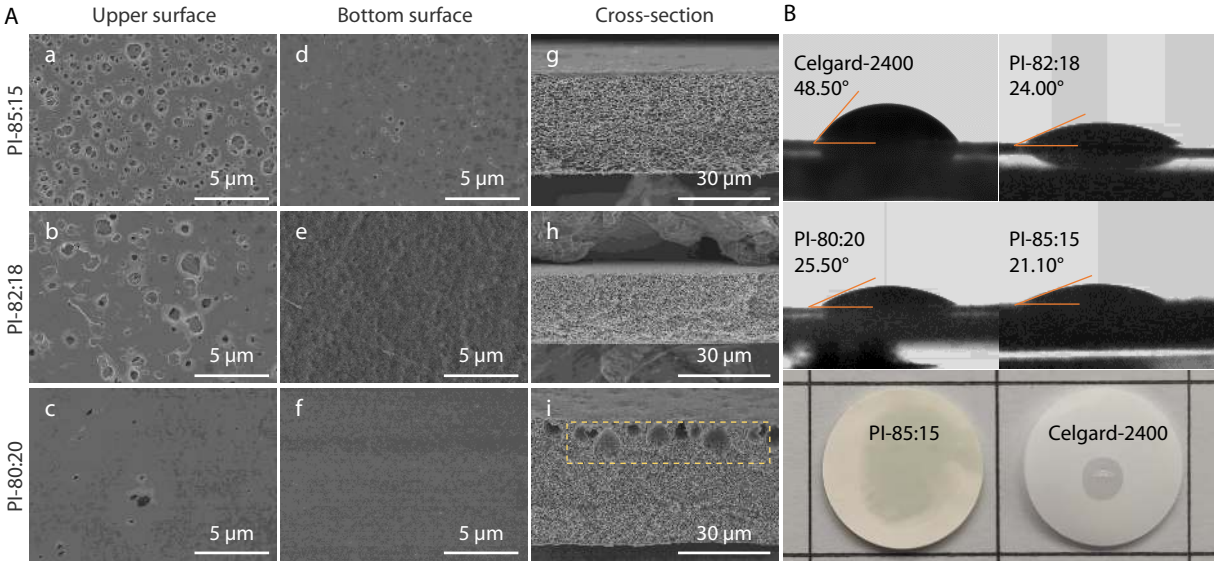

Fig. 3 (A) SEM images of PI separators, (a, b, c) top surface of separators, (d, e, f) bottom surface of separators, (g, h, i) cross-section of separators. (B) Electrolyte contact angles of PE and PI separators, photographs showing liquid electrolyte wetting behavior of PE and PI separators.

https://doi.org/10.1007/s10118-022-2678-4

Table 1 Thickness, porosities, ionic conductivities and electrolyte uptakes of the separators.

Separator	Thickness (μm)	Porosity (%)	Ion conductivity ($S \cdot cm^{-1}$)	Electrolyte uptake (%)
Celgard-2400	25	40.0	5.08×10^{-4}	134
PI-80:20	28±3	67.4	4.17×10^{-4}	256
PI-82:18	26±3	69.3	6.20×10^{-4}	304
PI-85:15	26±3	75.2	7.17×10^{-4}	344

thickness of the PI separator is controlled between 25–30 μm, specifically 28 μm (PI-80:20), 26 μm (PI-82:18) and 26 μm (PI-85:15), respectively, and when the proportion of NMP in the solidification bath increased, the porosity of the PI separators increased up to 75.2%. Meanwhile, the increase in separators porosity was accompanied by a gradual decrease in the mechanical strength of the separator (Fig. S3 in ESI), with the minimum tensile strength of 16.55 MPa for PI-85:15. As displayed in Fig. 3, the upper surface (the side in contact with the solidification bath) and the lower surface (the side in contact with the glass plate) of the separators showed different pore distributions, which could be attributed to the different rates of liquid-liquid phase separation in the different sections of the separators that the upper surface being the first to precipitate under a non-solvent solution while inhibiting phase separation in the lower section. Observing the upper surface morphology of the PI-85:15 separator, it can be seen that most of the pores are less than 1 μm, with a small proportion of pores above 1 μm present. These relatively large pores are not vertically through, but show a nested feature of large pores over small pores. The zigzagging interconnected pores facilitate the transportation of lithium ions and inhibit lithium dendrite formation.[39]

The wettability of the separators was also assessed by liquid electrolyte contact angle measurements. As shown in Fig. 3(B), the liquid electrolyte contact angle of the PE separator is 48.5°, which is higher than those of PI-80:20 (25.5°), PI-82:18 (24.0°) and PI-85:15 (21.1°) films. In fact, the excellent wettability of PI separators with liquid electrolytes can be contributed to the relative polarity of the imide component, which provided a higher surface polarity and allowed for more adequate wetting in liquid electrolytes.[45,46] At the same time, the dense sponge-like pore structure and higher porosity can store more liquid electrolyte, which facilitated the cycle and rate performance of lithium batteries.[47] As shown in Table 1, the PI-85:15 (344%) separator illustrates a higher electrolyte uptake than those of PI-80:20 (256%) and

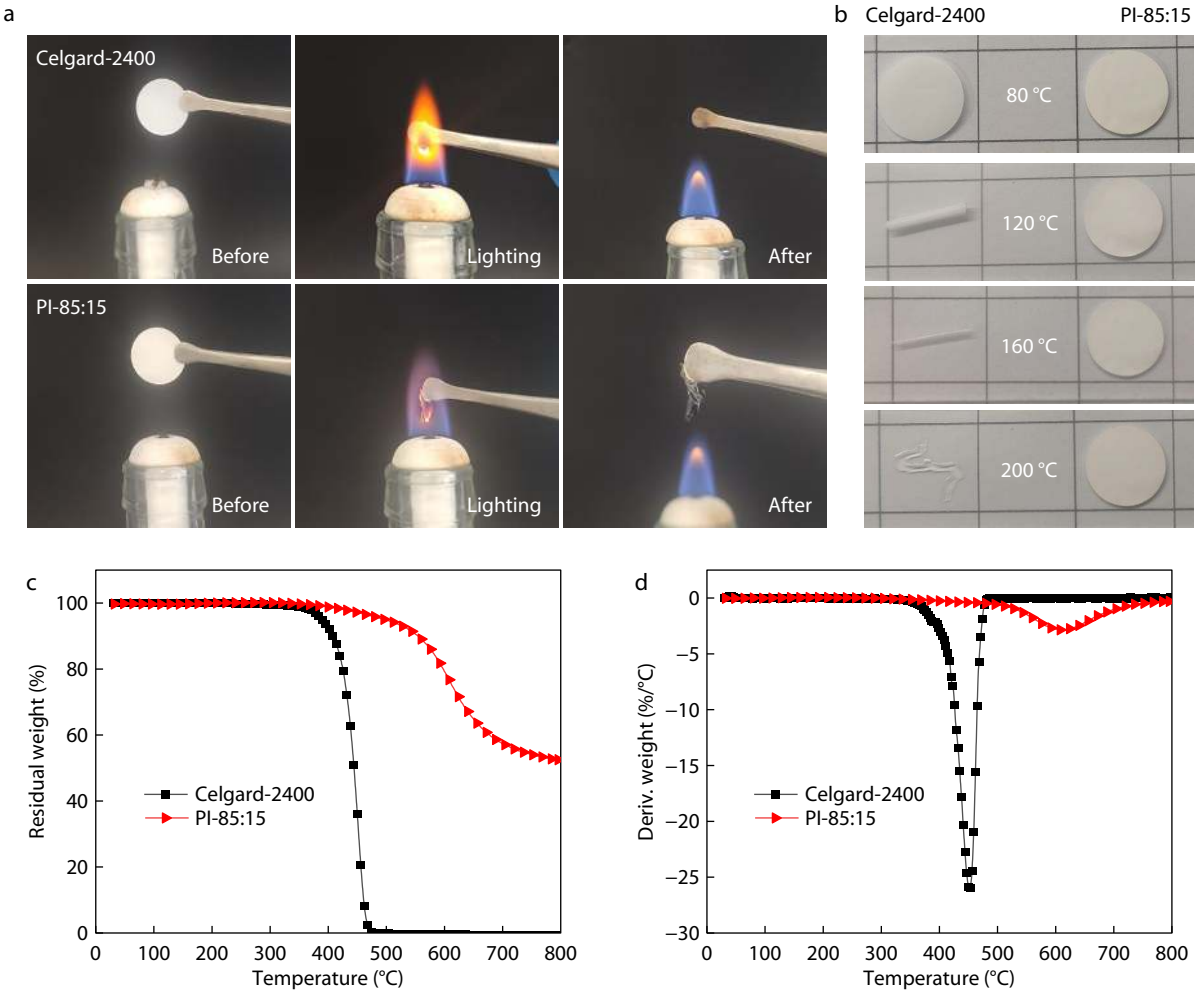

Fig. 4 (a) Flame-retardant properties and (b) thermal shrinkages of PI and Celgard separators; (c) TGA and (d) DTG curves of PI and Celgard separators.

https://doi.org/10.1007/s10118-022-2678-4

PI-82:18 (304%) separators, which is much higher than that of PE separator (134%).

Flame Retardant Properties and Thermal Stability

The flame retardancy properties of PI and Celgard separators were further evaluated by combustion tests. As shown in Fig. 4(a), Celgard separators immediately burn on contact with flame and decompose rapidly within a few seconds. In contrast, PI separators are non-flammable and self-extinguishing owing to the presence of a trifluoromethyl group (—CF_3) in the PI backbone, which gave the separator excellent flame retardancy.[48] Furthermore, thermal stability is one of the most significant factors affecting the safety performance of the battery. As shown in Fig. 4(b), the commercial Celgard series separators show severe shrinkage at 120 ℃ and completely melting with the temperature reaching 200 ℃. While PI separators maintain their dimensional integrity even at 200 ℃. The thermal stability of the separators was analyzed by TGA and DTG in N_2 atmosphere. As displayed in Fig. 4(c), PE separators started to decompose around 370 ℃. For PI separators, the TGA (Fig. 4c) and DTG (Fig. 4d) curves are relatively smooth until 350 ℃, the slight weight loss at 350–500 ℃ was attributed to the dehydration of the carboxyl groups reaction to acid anhydride, and the weight loss at 500–800 ℃ was attributed to the degradation of the PI molecule backbone. It is clear that PI separators demonstrating the excellent thermal stability. This highly heat-resistant separator could avoid the severe shrinkage that can occur when the battery was charged/discharged at high scan rates, which may lead to the thermal runaway even explosion.

Electrochemical Performances

The electrochemical stability of the separator in the electrolyte was assessed by linear scanning voltammetry (LSV) at room temperature. As shown in Fig. 5(a), Celgard 2400 separator shows no obvious change in current at voltages below 4.5 V, indicating that no significant oxidative decomposition of the separator occurred below 4.5 V versus Li^+/Li. The PI separator displays a similar window of electrochemical stability to the Celgard 2400 separator. The ionic conductivity of separators was investigated by electrochemical impedance spectroscopy. As exhibited in Fig. 5(b), the bulk resistances of the Celgard 2400, PI-80:20, PI-82:18 and PI-85:15 separators are 3.51, 3.43, 2.14 and 1.85 Ω, respectively, corresponding to the ionic conductivities of 5.08×10^{-4}, 4.17×10^{-4}, 6.20×10^{-4} and 7.17×10^{-4} S·cm^{-1}, respectively. PI-85:15 film possesses the highest ionic conductivity, not only due to the abundance of polar imide bonds, but also due to the highly porous pore structures.[49] Furthermore, the interfacial resistance of cells using Celgard 2400 and PI separators was measured for the assembled coin

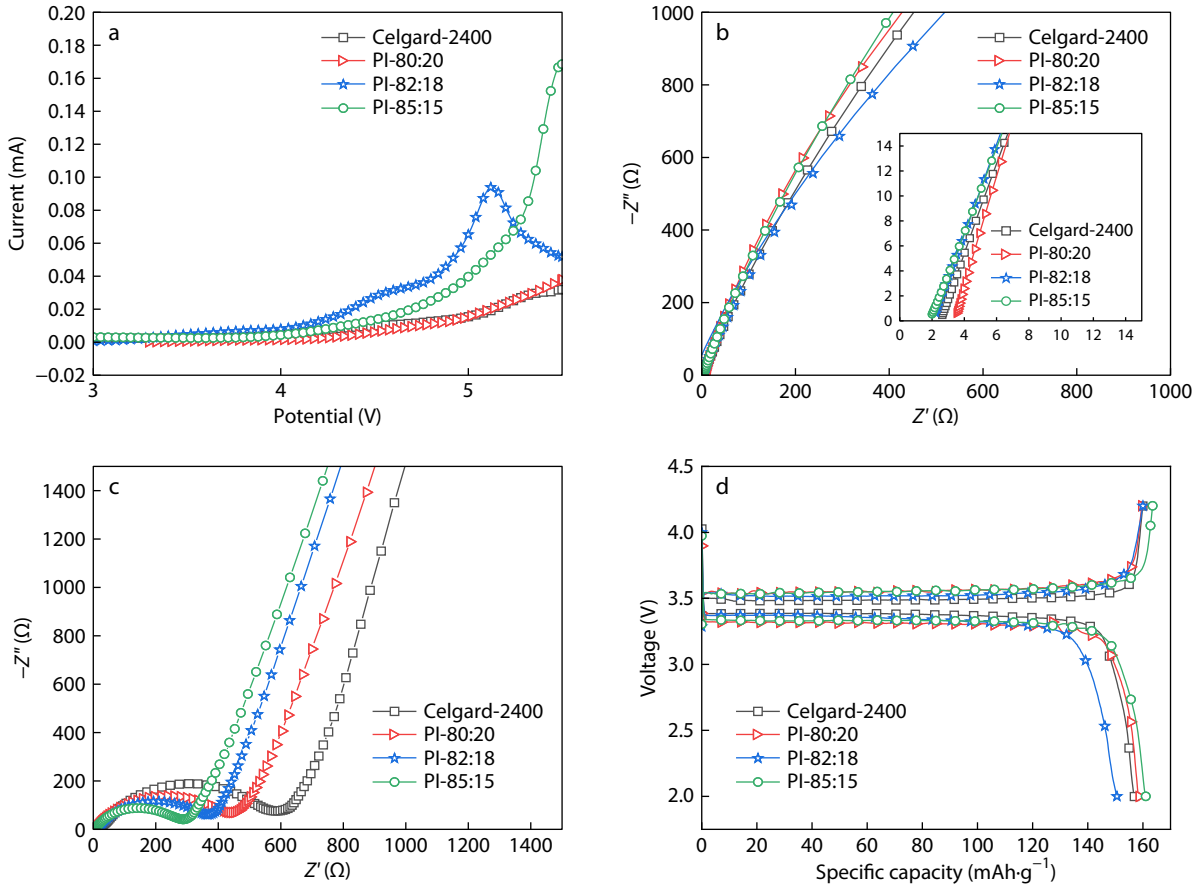

Fig. 5 (a) Linear sweep voltammograms of PI and Celgard separators; (b) Electrochemical impedance spectroscopy (EIS) of the cell with the PI and Celgard separators sandwiched between two stainless steels; (c) Nyquist plots of PI and Celgard separators using a Li/separator/$LiFePO_4$ configuration; (d) The first charge/discharge profiles of the half-cell with PI and Celgard separators at 0.2 C.

https://doi.org/10.1007/s10118-022-2678-4

cells. As shown in Fig. 5(c), the cell assembled by PI-85:15 separator shows the lowest interfacial resistance, which could be attributed to the excellent interface compatibility between the high-porosity separator and the liquid electrolyte. Fig. 5(d) displays the first charge/discharge curves of cells with Celgard 2400 separator and PI separators at 0.2 C, from which it can be seen that the cells with PI separators had a stable charge/discharge curve and a smooth charge/discharge plateau, which was similar to that of Celgard separator, demonstrating the stable electrochemical properties of as-prepared PI films.

Li^+ transport properties have a major impact on the battery performance and the Li^+ transfer number could be calculated by a combination of the chronoamperometry and AC impedance analysis. As shown in Fig. 6 and Table 1, the obtained Li^+ transfer numbers (t_{Li^+}) for PI-82:18 and PI-85:15 separators are 0.43 and 0.48, respectively, which are higher than that of Celgard 2400 (0.38). The facilitated Li^+ transport properties could be ascribed to the high porosity of PI separators with more transport channels providing for Li^+ ions. Besides, the deliberated —COOH groups containing non-shared electron pairs can also interact with the solvated lithium ions to realize the desolvation of Li^+ ions and improve the transport rate.[41] To further confirm the effect of —COOH groups on the transport properties of Li^+ ions, PI film with and without —COOH groups (Fig. S4 in ESI) were synthesized. The separators were formed under the same solidification bath conditions (NMP/H_2O=85/15). It is clear that the separator containing —COOH groups have a higher Li^+ transfer number (0.39) than that of without —COOH groups (0.36). Meanwhile, it can be noticed that the Li^+ transfer number increased with the increase of the carboxyl contents of the separator. As exhibited in Fig. 6(d), compared with some results in reported work, the obtained PI-85:15 separator shows superior performance of ionic conductivity, electrolyte uptake and Li^+ transfer numbers, which could be ascribed to the unique designed chemical structures and spongy porous microstructures.

Fig. 7(a) displays the cycling performance of the cells with different separators for 200 cycles at a current density of 1 C. The cell with PI-80:20 as separator failed after one or two cycles probably due to the presence of large porous structures which caused lithium dendrites piercing the separator easily. When the $LiFePO_4$/Li cells were cycled to the 20th turn, the cells assembled with PI-82:18 and PI-85:15 separators show discharge capacities of 149.3 and 151.2 mA·h·g^{-1}, respectively, which are higher than that of the cells with Celgard 2400 (142.1 mA·h·g^{-1}). After 200 cycles, $LiFePO_4$/Li cells with Celgard 2400, PI-82:18 and PI-85:15 separators reflect high discharge capacities of 126.7, 130 and 135.1 mA·h·g^{-1}, with

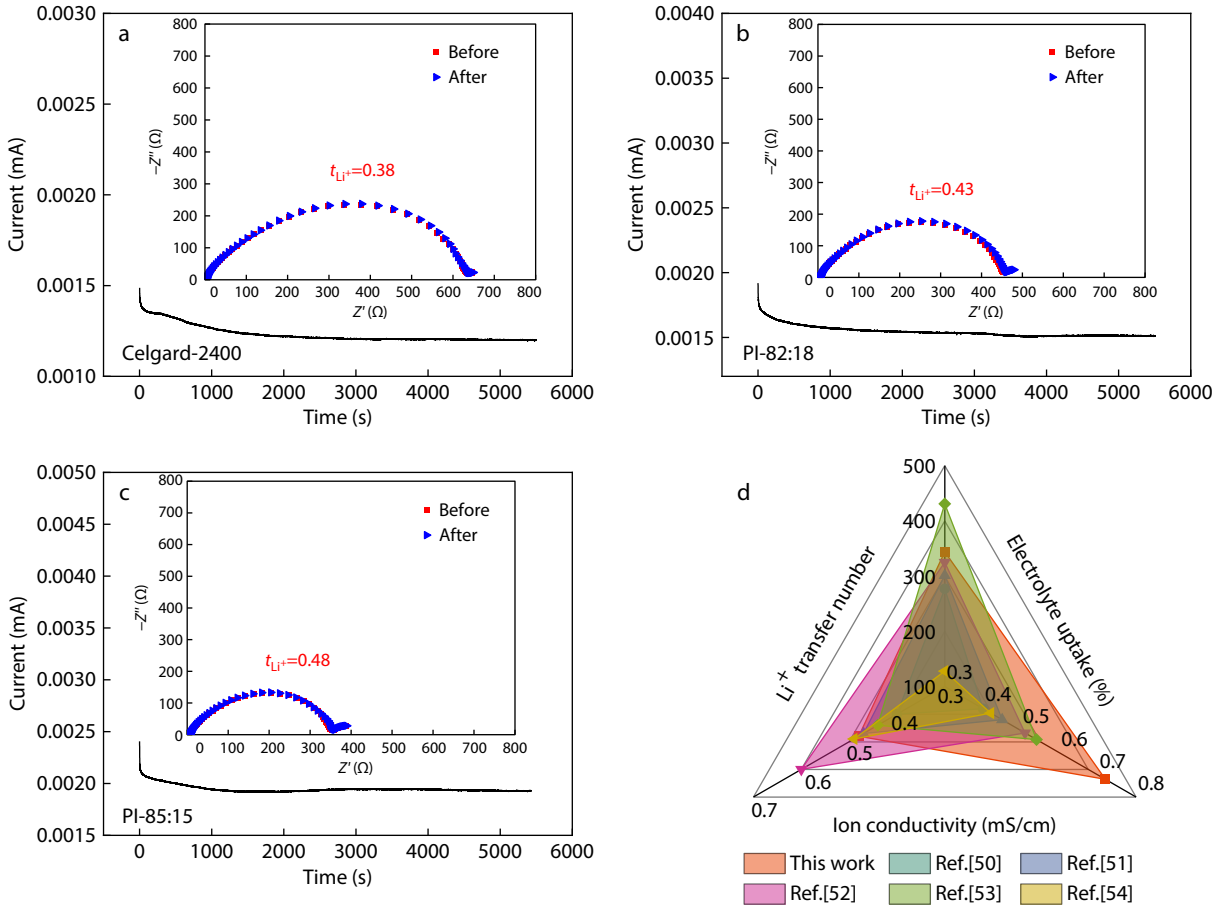

Fig. 6 (a, b, c) Chronoamperometry profiles and EIS of Li/electrolyte-soaked separator/Li cells. (Inset: EIS for the same cells before and after polarization), (d) The comparison of ionic conductivity, lithium ion transfer number and electrolyte uptake of separators in this work and other literature (Ref. [50], Ref. [51], Ref. [52], Ref. [53], Ref. [54]).

https://doi.org/10.1007/s10118-022-2678-4

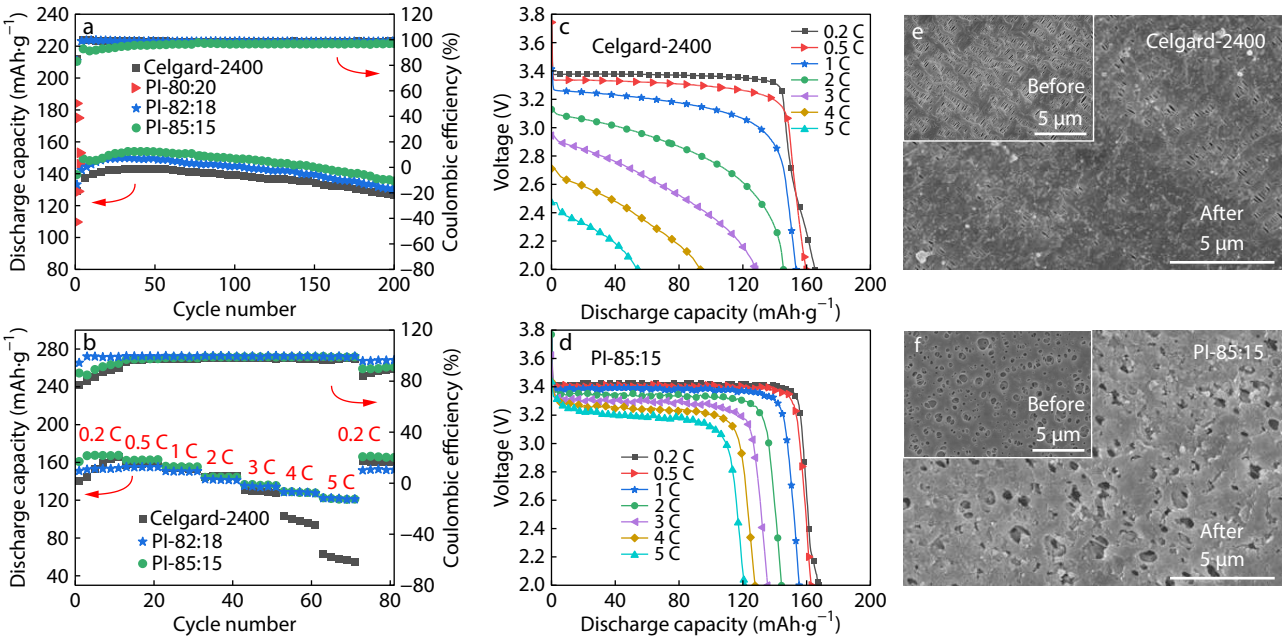

Fig. 7 (a) The cycle performance and (b) rate capability of the cells assembled with the PI and Celgard separators; Discharge profiles of cells assembled with Celgard 2400 (c) and PI-85:15 (d) separators at various current densities, the SEM images of Celgard 2400 (e) and PI-85:15 (f) after 200 cycles. (Inset: SEM images for the same separator before the cycle)

the capacity retention of 89.16%, 87.07% and 89.35%, respectively. In addition, the coulomb efficiencies all remained above 98% after 200 cycles. The SEM images of the separators before and after 200 cycles are shown in Figs. 7(e) and 7(f). It is clear that the more pores the PI separator has, the more pores it could retain after 200 cycles. The good cycle performance of PI separators is based on the high electrolyte uptake of PI separators, which helps to reduce electrolyte leakage. Furthermore, high porosity of the PI separators facilitates the storage of more electrolyte and the unique sponge-like pore structure prevents the growth of lithium dendrites, thereby improving the cycling stability.[55] The rate performances of the cells with PI separators and Celgard 2400 separator were exhibited in Fig. 7(b). The cell with PI-85:15 separator showed specific capacities of 167.3, 162.5, 155.5, 144.3, 136.6, 129.1 and 121.8 mA·h·g^{-1} at the scan rates of 0.2, 0.5, 1, 2, 3, 4 and 5 C, respectively. When the current density subsequently returned from 5 C to 0.2 C, the discharge specific capacity can retain 165.5 mA·h·g^{-1} with the recovery rate of 98.92% for specific capacity, demonstrating the excellent rate performance. Moreover, the discharge capacity of the cell with the Celgard 2400 separator dropped considerably at the scan rates of 4 and 5 C with a discharge capacity of 54.3 mA·h·g^{-1} at 5 C as shown in Fig. 7(c). While the cell assembled with PI-85:15 separator could reach a high discharge capacity of 121.8 mA·h·g^{-1} at 5 C (Fig. 7d). The good rate performance of PI-85:15 separator could be attributed to their high porosity, large electrolyte uptake, fast Li^+ transport properties and high ionic conductivity.[56]

CONCLUSIONS

In summary, soluble PIs bearing functional groups were synthesized by molecular structural design and the porous PI separators were prepared *via* non-solvent induced phase separation. Various porous PI separators with different morphologies were obtained by regulating the NMP/water ratios in the solidification bath. With 82% and 85% content of NMP in the solidification bath, PI separators with interconnected and spongy porous structures were obtained, which could maintain dimensional integrity even at 200 °C and exhibit excellent fire resistance and thermal stability. The high porosity of the PI separators and the presence of polar imide bonds in the molecular structure provided excellent electrolyte wettability with the electrolyte uptake of 344%. At the same time, the —COOH groups containing unshared electron pairs promoted the Li^+ transfer and increased the lithium-ion transference number. These advantages lead to a significant improvement in the electrochemical properties for the cell assembled with PI separators, which displayed a discharge specific capacity of 135.1 mA·h·g^{-1} after 200 cycles, a capacity retention rate of 89.35%, and a discharge specific capacity of 121.80 mA·h·g^{-1} at a rate of 5 C, demonstrating the great potential of PI separators for charging and discharging at high rates. The results of this study show that polyimide separators based on functional groups hold great promise for high safety and high-performance LIBs.

NOTES

The authors declare no competing financial interest.

Electronic Supplementary Information

Electronic supplementary information (ESI) is available free of

charge in the online version of this article at http://doi.org/10.1007/s10118-022-2678-4.

ACKNOWLEDGMENTS

This work was financially supported by the National Natural Science Foundation of China (Nos. U21A2087, 51903038 and 21975040).

REFERENCES

1 Shan, X. Y.; Li, F.; Wang, D. W.; Cheng, H. M. The smart era of electrochemical energy storage devices. *Energy Storage Mater.* **2016**, *3*, 66–68.
2 Lee, H.; Yanilmaz, M.; Toprakci, O.; Fu, K.; Zhang, X. A review of recent developments in membrane separators for rechargeable lithium-ion batteries. *Energy Environ. Sci.* **2014**, *7*, 3857–3886.
3 Li, Y.; Yu, L.; Hu, W.; Hu, X. Thermotolerant separators for safe lithium-ion batteries under extreme conditions. *J. Mater. Chem. A* **2020**, *8*, 20294–20317.
4 Feng, X.; Ouyang, M.; Liu, X.; Lu, L.; Xia, Y.; He, X. Thermal runaway mechanism of lithium ion battery for electric vehicles: a review. *Energy Storage Mater.* **2018**, *10*, 246–267.
5 Shin, D. W.; Guiver, M. D.; Lee, Y. M. Hydrocarbon-based polymer electrolyte membranes: importance of morphology on ion transport and membrane stability. *Chem. Rev.* **2017**, *117*, 4759–4805.
6 Li, D.; Zhang, H.; Li, X. Porous polyetherimide membranes with tunable morphology for lithium-ion battery. *J. Membr. Sci.* **2018**, *565*, 42–49.
7 Yin, M.; Huang, J.; Yu, J.; Chen, G.; Qu, S.; Wang, X.; Li, C. The polypropylene membrane modified by an atmospheric pressure plasma jet as a separator for lithium-ion button battery. *Electrochim. Acta* **2018**, *260*, 489–497.
8 Costa, C. M.; Lee, Y. H.; Kim, J. H.; Lee, S. Y.; Lanceros- Méndz, S. Recent advances on separator membranes for lithium-ion battery applications: from porous membranes to solid electrolytes. *Energy Storage Mater.* **2019**, *22*, 346–375.
9 Heidari, A. A.; Mahdavi, H. Recent development of polyolefin-based microporous separators for Li-ion batteries: a review. *Chem. Rec.* **2020**, *20*, 570–595.
10 Gu, Q. Q.; Xue, H. J.; Li, Z. W.; Song, J. C.; Sun, Z. Y. High-performance polyethylene separators for lithium-ion batteries modified by phenolic resin. *J. Power Sources* **2021**, *483*, 229155.
11 Sheng, L.; Song, L.; Gong, H.; Pan, J.; Bai, Y.; Song, S.; Liu, G.; Wang, T.; Huang, X.; He, J. Polyethylene separator grafting with polar monomer for enhancing the lithium-ion transport property. *J. Power Sources* **2020**, *479*, 228812.
12 Luo, W.; Cheng, S.; Wu, M.; Zhang, X.; Yang, D.; Rui, X. A review of advanced separators for rechargeable batteries. *J. Power Sources* **2021**, *509*, 230372.
13 Ding, L.; Zhang, C.; Wu, T.; Yang, F.; Lan, F.; Cao, Y.; Xiang, M. Effect of temperature on compression behavior of polypropylene separator used for Lithium-ion battery. *J. Power Sources* **2020**, *466*, 228300.
14 Feng, X.; Zheng, S.; Ren, D.; He, X.; Wang, L.; Cui, H.; Liu, X.; Jin, C.; Zhang, F.; Xu, C.; Hsu, H.; Gao, S.; Chen, T.; Li, Y.; Wang, T.; Wang, H.; Li, M.; Ouyang, M. Investigating the thermal runaway mechanisms of lithium-ion batteries based on thermal analysis database. *Appl. Energy* **2019**, *246*, 53–64.
15 Lu, L.; Han, X.; Li, J.; Hua, J.; Ouyang, M. A review on the key issues for lithium-ion battery management in electric vehicles. *J. Power Sources* **2013**, *226*, 272–288.
16 Orendorff, C. J.; Lambert, T. N.; Chavez, C. A.; Bencomo, M.; Fenton, K. R. Polyester separators for lithium-ion cells: improving thermal stability and abuse tolerance. *Adv. Energy Mater.* **2013**, *3*, 314–320.
17 Song, J.; Ryou, M. H.; Son, B.; Lee, J. N.; Lee, D. J.; Lee, Y. M.; Choi, J. W.; Park, J. K. Co-polyimide-coated polyethylene separators for enhanced thermal stability of lithium ion batteries. *Electrochim. Acta* **2012**, *85*, 524–530.
18 Liang, N.; Fang, J.; Guo, X. A simple approach for preparation of porous polybenzimidazole membranes as a promising separator for lithium ion batteries. *J. Mater. Chem. A* **2017**, *5*, 15087–15095.
19 Liu, X.; Wu, Y.; Yang, F.; Wang, S.; Zhang, B.; Wang, L. An effective dual-channel strategy for preparation of polybenzimidazole separator for advanced-safety and high-performance lithium-ion batteries. *J. Membr. Sci.* **2021**, *626*, 119190.
20 Liu, X.; Zhang, B.; Wu, Y.; Chen, J.; Fang, M.; Wang, L.; Wang, L. The effects of polybenzimidazole nanofiber separator on the safety and performance of lithium-ion batteries: characterization and analysis from the perspective of mechanism. *J. Power Sources* **2020**, *475*, 228624.
21 Patel, A.; Wilcox, K.; Li, Z.; George, I.; Juneja, R.; Lollar, C.; Lazar, S.; Grunlan, J.; Tenhaeff, W. E.; Lutkenhaus, J. L. High modulus, thermally stable, and self-extinguishing aramid nanofiber separators. *ACS Appl. Mater. Interfaces* **2020**, *12*, 25756–25766.
22 Yang, B.; Wang, L.; Zhang, M.; Li, W.; Zhou, Q.; Zhong, L. Advanced separators based on aramid nanofiber (ANF) membranes for lithium-ion batteries: a review of recent progress. *J. Mater. Chem. A* **2021**, *9*, 12923–12946.
23 Liu, J.; Wang, J.; Zhu, L.; Chen, X.; Ma, Q.; Wang, L.; Wang, X.; Yan, W. A high-safety and multifunctional MOFs modified aramid nanofiber separator for lithium-sulfur batteries. *Chem. Eng. J.* **2021**, *411*, 128540.
24 l'Abee, R.; DaRosa, F.; Armstrong, M. J.; Hantel, M. M.; Mourzagh, D. High temperature stable Li-ion battery separators based on polyetherimides with improved electrolyte compatibility. *J. Power Sources Sources* **2017**, *345*, 202–211.
25 Shi, J.; Xia, Y.; Yuan, Z.; Hu, H.; Li, X.; Zhang, H.; Liu, Z. Porous membrane with high curvature, three-dimensional heat-resistance skeleton: a new and practical separator candidate for high safety lithium ion battery. *Sci. Rep.* **2015**, *5*, 8255.
26 Kong, L.; Liu, B.; Ding, J.; Yan, X.; Tian, G.; Qi, S.; Wu, D. Robust polyetherimide fibrous membrane with crosslinked topographies fabricated *via in-situ* micro-melting and its application as superior Lithium-ion battery separator with shutdown function. *J. Membr. Sci.* **2018**, *549*, 244–250.
27 Qi, W.; Lu, C.; Chen, P.; Han, L.; Yu, Q.; Xu, R. Electrochemical performances and thermal properties of electrospun poly(phthalazinone ether sulfone ketone) membrane for lithium-ion battery. *Mater. Lett.* **2012**, *66*, 239–241.
28 Wang, T.; Sun, F.; Wang, H.; Yang, S.; Fan, L. Preparation and properties of pore-filling membranes based on sulfonated copolyimides and porous polyimide matrix. *Polymer* **2012**, *53*, 3154–3162.
29 Pai, J. Y.; Hsieh, C. T.; Lee, C. H.; Wang, J. A.; Ku, H. Y.; Huang, C. L.; Hardwick, L. J.; Hu, C. C. Engineering of electrospun polyimide separators for electrical double-layer capacitors and lithium-ion cells. *J. Power Sources* **2021**, *482*, 229054.
30 Lin, D.; Zhuo, D.; Liu, Y.; Cui, Y. All-integrated bifunctional separator for Li dendrite detection *via* novel solution synthesis of a thermostable polyimide separator. *J. Am. Chem. Soc.* **2016**, *138*, 11044–11050.
31 Liao, C.; Wang, W.; Wang, J.; Han, L.; Qiu, S.; Song, L.; Gui, Z.; Kan, Y.; Hu, Y. Magnetron sputtering deposition of silicon nitride on polyimide separator for high-temperature lithium-ion batteries. *J. Energy Chem.* **2021**, *56*, 1–10.
32 Lu, Z.; Sui, F.; Miao, Y. E.; Liu, G.; Li, C.; Dong, W.; Cui, J.; Liu, T.; Wu,

J.; Yang, C. Polyimide separators for rechargeable batteries. *J. Energy Chem.* **2021**, *58*, 170–197.
33 Dong, G.; Liu, B.; Kong, L.; Wang, Y.; Tian, G.; Qi, S.; Wu, D. Neoteric polyimide nanofiber encapsulated by the TiO_2 armor as the tough, highly wettable, and flame-retardant separator for advanced lithium-ion batteries. *ACS Sustain. Chem. Eng.* **2019**, *7*, 17643–17652.
34 Huang, X.; Hitt, J. Lithium ion battery separators: development and performance characterization of a composite membrane. *J. Membr. Sci.* **2013**, *425-426*, 163-168.
35 Shi, C.; Zhang, P.; Huang, S.; He, X.; Yang, P.; Wu, D.; Sun, D.; Zhao, J. Functional separator consisted of polyimide nonwoven fabrics and polyethylene coating layer for lithium-ion batteries. *J. Power Sources* **2015**, *298*, 158–165.
36 Yu, B. C.; Park, K.; Jang, J. H.; Goodenough, J. B. Cellulose-based porous membrane for suppressing Li dendrite formation in lithium-sulfur battery. *ACS Energy Lett.* **2016**, *1*, 633–637.
37 Shi, J.; Hu, H.; Xia, Y.; Liu, Y.; Liu, Z. Polyimide matrix-enhanced cross-linked gel separator with three-dimensional heat-resistance skeleton for high-safety and high-power lithium ion batteries. *J. Mater. Chem. A* **2014**, *2*, 9134–9141.
38 Tan, J.; Kong, L.; Qiu, Z.; Yan, Y. Flexible, high-wettability and thermostable separator based on fluorinated polyimide for lithium-ion battery. *J. Solid State Electrochem.* **2018**, *22*, 3363–3373.
39 Zhang, H.; Lin, C. E.; Zhou, M. Y.; John, A. E.; Zhu, B. K. High thermal resistance polyimide separators prepared *via* soluble precusor and non-solvent induced phase separation process for lithium ion batteries. *Electrochim. Acta* **2016**, *187*, 125–133.
40 Li, D.; Wang, H.; Luo, L.; Zhu, J.; Li, J.; Liu, P.; Yu, Y.; Jiang, M. Electrospun separator based on sulfonated polyoxadiazole with outstanding thermal stability and electrochemical properties for lithium-ion Batteries. *ACS Appl. Energy Mater.* **2021**, *4*, 879–887.
41 Lin, C. E.; Zhang, H.; Song, Y. Z.; Zhang, Y.; Yuan, J. J.; Zhu, B. K. Carboxylated polyimide separator with excellent lithium ion transport properties for a high-power density lithium-ion battery. *J. Mater. Chem. A* **2018**, *6*, 991–998.
42 Dhara, M. G.; Banerjee, S. Fluorinated high-performance polymers: poly(arylene ether)s and aromatic polyimides containing trifluoromethyl groups. *Prog. Polym. Sci.* **2010**, *35*, 1022–1077.
43 Zhai, L.; Yang, S.; Fan, L. Preparation and characterization of highly transparent and colorless semi-aromatic polyimide films derived from alicyclic dianhydride and aromatic diamines. *Polymer* **2012**, *53*, 3529–3539.
44 Qiu, W.; Chen, C. C.; Xu, L.; Cui, L.; Paul, D. R.; Koros, W. J. Sub-T_g cross-linking of a polyimide membrane for enhanced CO_2 plasticization resistance for natural gas separation. *Macromolecules* **2011**, *44*, 6046–6056.
45 Shi, J. L.; Fang, L. F.; Li, H.; Zhang, H.; Zhu, B. K.; Zhu, L. P. Improved thermal and electrochemical performances of PMMA modified PE separator skeleton prepared *via* dopamine-initiated ATRP for lithium ion batteries. *J. Membr. Sci.* **2013**, *437*, 160–168.
46 Miao, Y. E.; Zhu, G. N.; Hou, H.; Xia, Y. Y.; Liu, T. Electrospun polyimide nanofiber-based nonwoven separators for lithium-ion batteries. *J. Power Sources* **2013**, *226*, 82–86.
47 Kong, L.; Yan, Y.; Qiu, Z.; Zhou, Z.; Hu, J. Robust fluorinated polyimide nanofibers membrane for high-performance lithium-ion batteries. *J. Membr. Sci.* **2018**, *549*, 321–331.
48 Luo, X.; Lu, X.; Chen, X.; Chen, Y.; Song, C.; Yu, C.; Wang, N.; Su, D.; Wang, C.; Gao, X.; Wang, G.; Cui, L. A robust flame retardant fluorinated polyimide nanofiber separator for high-temperature lithium-sulfur batteries. *J. Mater. Chem. A* **2020**, *8*, 14788–14798.
49 Hussain, A.; Li, D.; Luo, Y.; Zhang, H.; Zhang, H.; Li, X. Porous membrane with improved dendrite resistance for high-performance lithium metal-based battery. *J. Membr. Sci.* **2020**, *605*, 118108.
50 Wang, Q.; Yang, J.; Wang, Z.; Shi, L.; Zhao, Y.; Yuan, S. Dual-scale Al_2O_3 particles coating for high-performance separator and lithium metal anode. *Energy Technol.* **2020**, *8*, 1901429.
51 Wang, Y.; Shi, L.; Zhou, H.; Wang, Z.; Li, R.; Zhu, J.; Qiu, Z.; Zhao, Y.; Zhang, M.; Yuan, S. Polyethylene separators modified by ultrathin hybrid films enhancing lithium ion transport performance and Li-metal anode stability. *Electrochim. Acta* **2018**, *259*, 386–394.
52 Xu, W.; Wang, Z.; Shi, L.; Ma, Y.; Yuan, S.; Sun, L.; Zhao, Y.; Zhang, M.; Zhu, J. Layer-by-layer deposition of organic-inorganic hybrid multilayer on microporous polyethylene separator to enhance the electrochemical performance of lithium-ion battery. *ACS Appl. Mater. Interfaces* **2015**, *7*, 20678–20686.
53 Mao, X.; Shi, L.; Zhang, H.; Wang, Z.; Zhu, J.; Qiu, Z.; Zhao, Y.; Zhang, M.; Yuan, S. Polyethylene separator activated by hybrid coating improving Li^+ ion transference number and ionic conductivity for Li-metal battery. *J. Power Sources* **2017**, *342*, 816–824.
54 Song, Y. Z.; Yuan, J. J.; Yin, X.; Zhang, Y.; Lin, C. E.; Sun, C. C.; Fang, L. F.; Zhu, B.; Zhu, L. P. Effect of polyphenol-polyamine treated polyethylene separator on the ionic conduction and interface properties for lithium-metal anode batteries. *J. Electroanal. Chem.* **2018**, *816*, 68–74.
55 Li, D.; Shi, D.; Xia, Y.; Qiao, L.; Li, X.; Zhang, H. Superior thermally stable and nonflammable porous polybenzimidazole membrane with high wettability for high-power lithium-ion batteries. *ACS Appl. Mater. Interfaces* **2017**, *9*, 8742–8750.
56 Zhang, Y.; Wang, Z.; Xiang, H.; Shi, P.; Wang, H. A thin inorganic composite separator for lithium-ion batteries. *J. Membr. Sci.* **2016**, *509*, 19–26.

https://doi.org/10.1007/s10118-022-2678-4